

Spitzer IRS Spectra of Luminous 8 μm Sources in the Large Magellanic Cloud: Testing color-based classifications

Catherine L. Buchanan¹, Joel H. Kastner², Bruce J. Hrivnak³, Raghvendra Sahai⁴

ABSTRACT

We present archival *Spitzer* IRS spectra of 19 luminous 8 μm selected sources in the Large Magellanic Cloud (LMC). The object classes derived from these spectra and from an additional 24 spectra in the literature are compared with classifications based on 2MASS/MSX (J, H, K, and 8 μm) colors in order to test the “JHK8” classification scheme (Kastner et al. 2008). The IRS spectra confirm the classifications of 22 of the 31 sources that can be classified under the JHK8 system. The spectroscopic classification of 12 objects that were unclassifiable in the JHK8 scheme allow us to characterize regions of the color-color diagrams that previously lacked spectroscopic verification, enabling refinements to the JHK8 classification system. The results of these new classifications are consistent with previous results concerning the identification of the most infrared-luminous objects in the LMC. In particular, while the IRS spectra reveal several new examples of asymptotic giant branch (AGB) stars with O-rich envelopes, such objects are still far outnumbered by carbon stars (C-rich AGB stars). We show that *Spitzer* IRAC/MIPS color-color diagrams provide improved discrimination between red supergiants and oxygen-rich and carbon-rich asymptotic giant branch stars relative to those based on 2MASS/MSX colors. These diagrams will enable the most luminous IR sources in Local Group galaxies to be classified with high confidence based on their *Spitzer* colors. Such characterizations of stellar populations will continue to be possible during *Spitzer*’s warm mission, through the use of IRAC [3.6]-[4.5] and 2MASS colors.

Subject headings: circumstellar matter — infrared: stars — Magellanic Clouds — stars:AGB and post-AGB — stars: mass loss

1. INTRODUCTION

The infrared wavelength regime is key to understanding the early and late stages of stellar evolution, which are characterized by circumstellar dust. Objects in these phases should dominate

¹School of Physics, University of Melbourne, Parkville, Victoria, 3010 Australia. Email: clb@unimelb.edu.au

²Center for Imaging Science, Rochester Institute of Technology, 54 Lomb Memorial Drive, Rochester NY 14623. Presently Visiting Astronomer, LAOG, Grenoble.

³Dept. of Physics and Astronomy, Valparaiso University, Valparaiso, IN 46383

⁴NASA/JPL, 4800 Oak Grove Drive, Pasadena, CA 91109

the mid-infrared (MIR) point source populations of nearby galaxies. The *Spitzer* Space Telescope has enabled the detection of large numbers of mass-losing evolved stars and dust-enshrouded young stellar objects throughout the Local Group (e.g., Blum et al. 2006; Jackson et al. 2006, 2007; Cannon et al. 2006). Identification of these objects relies on their location in color-color and color-magnitude diagrams, and is often based on stellar evolution models (e.g., Blum et al. 2006). Reliable classification of objects based on photometry requires spectroscopic confirmation. Such confirmation is especially important when attempting to distinguish between the various classes of very highly obscured (and hence IR-luminous) mass-losing evolved stars, such as red supergiants vs. asymptotic giant branch (AGB) stars, and AGB stars with oxygen-rich vs. carbon-rich circumstellar envelopes. These determinations in turn provide key input for models of galactic chemical enrichment.

This paper is the third in our series discussing the classification of compact IR-luminous sources in the Large Magellanic Cloud (LMC). Our sample was selected from the sample of >1650 2MASS/MSX LMC sources compiled by Egan, Van Dyk & Price (2001) (hereafter EVP01), and comprises the 250 luminous $8\ \mu\text{m}$ sources ($F_{8.3\ \mu\text{m}} > 150\ \text{mJy}$) that are not already known to be main sequence stars or Galactic objects (Kastner et al. 2008; hereafter Paper II). In Buchanan et al. (2006, hereafter Paper I), we classified and analyzed the *Spitzer* IRS¹ (Houck et al. 2004) spectra of 60 sources in our sample and derived spectroscopically verified color-color diagnostics using 2MASS and MSX A-band photometry. We refer to this 2MASS/MSX color-color classification system as the JHK8 scheme. In Paper II we classified >70% of the sample with high confidence, based on the JHK8 color-based classifications supplemented by data from the literature. In this paper, we use additional IRS spectra available from the *Spitzer* archive to further refine the JHK8 scheme and discuss classifications based on *Spitzer* photometry.

Of the sample of 250 luminous $8\ \mu\text{m}$ sources in the LMC, IRS spectra are available for 123 objects. Classifications for 60 of these were presented in Paper I. This paper presents classifications for 44 of the remaining 63 objects, which are listed in Table 1. The final 19 archival sources, which were not yet public at the time of submission of this paper, will be considered in a future paper. In §2, we discuss the data reduction for 20 of the 44 sources. The remaining 24 sources have spectra that are previously published in Speck et al. (2006), Zijlstra et al. (2006), and Sloan et al. (2008). We use the published spectra to do our own independent classification. In §3, we provide spectral classifications for these 44 sources (Table 2), which break down into the following categories and subcategories: 17 O-rich objects (3 AGB stars, 3 OH/IR stars, 4 B[e] stars, and 7 RSGs), 19 C-rich objects (all AGB stars), 4 H II regions, 3 Young Stellar Objects (YSOs) or candidate YSOs, and 1 unclassified source (spectrum too weak). We present the spectra for 9 new O-rich sources, 4 new C-rich sources, 4 new H II regions, and 2 candidate YSOs. In §4, we use these 44 sources to test and refine the JHK8 scheme. We find that 22 were classified correctly, 9 were not classified

¹The IRS was a collaborative venture between Cornell University and Ball Aerospace Corporation funded by NASA through the Jet Propulsion Laboratory and Ames Research Center.

correctly, 12 could not be classified with the JHK8 scheme, and 1 source had a spectrum too weak to classify. We describe revisions to this classification scheme based on these results, and extend the classifications to *Spitzer* IRAC/MIPS colors. We conclude with a summary in §5.

2. SAMPLE AND DATA REDUCTION

The selection of the sample is described briefly in §1 and more fully in Paper II. Table 1 lists the archival sample objects and the properties of the data. We note whether the data are publicly available as of the time of submission of this paper and list references where the data have appeared in the literature.

Table 1. Archival data sample

MSX LMC ^a	SIMBAD Name ^b	RA (J2000) ^c	Dec (J2000) ^c	Target Name ^d	PID ^e	AORKEY ^f	Public?	Ref. ^g
21	IRAS 05053-6659	05 05 20.35	-66 55 06.6	Cluster-013	40650	23893504	N	
43	HV 888	05 04 14.11	-67 16 14.5	HV 888	200	6015488	Y	S08
44	IRAS 05112-6755	05 11 10.42	-67 52 10.6	TRM4	3505	12939008	Y	Z06
46	LHA 120-N 17A	05 03 54.53	-67 18 48.6	SSTISAGE1C J050354.56-671848.5	40159	24317696	Y	
47	MXS LMC 47	05 11 13.85	-67 36 16.2	TRM24	3505	12937984	Y	Z06
80	EQ 051005.7-685634	05 09 51.70	-68 53 05.6	lmc-hii-86	40159	22470400	N	
134	HD 269006	05 02 07.39	-71 20 13.1	HD269006	1404	9108736	Y	
196	IRAS 05125-7035	05 12 00.82	-70 32 24.0	LI-LMC 0603	1094	6078464	Y	
198	HD 269211	05 12 30.17	-70 24 22.3	HD 269211	30869	19151360	Y	
215	LHA 120-N 113A	05 13 21.74	-69 22 39.4	Cluster-005	40650	23883008	N	
219	MSX LMC 219	05 11 19.46	-68 42 27.7	MSX051119.5-684227	3505	12939264	Y	Z06
223	LI-LMC 623	05 12 51.05	-69 37 50.5	MSX051250.8-693749	3505	12938752	Y	Z06
262	HD 34664	05 13 52.99	-67 26 54.6	HD 34664	30869	19149056	Y	
283	IRAS 05128-6455	05 13 04.56	-64 51 40.3	05128-6455	200	6024192	Y	S08
307	IRAS 05190-6748	05 18 56.28	-67 45 04.7	TRM20	3505	12938496	Y	Z06
318	IRAS 05195-6911	05 19 12.31	-69 09 06.5	Cluster-002	40650	23884288	N	
323	ARDB 184	05 16 31.80	-68 22 09.1	LHA 120-S 93	30869	19149312	Y	
341	MSX LMC 341	05 21 00.43	-69 20 55.3	MSX052100.5-692054	3505	12937728	Y	Z06
349	MSX LMC 349	05 17 26.98	-68 54 58.7	MSX051726.9-685458	3505	12938240	Y	Z06
356	2MASS J05190229-6938033	05 19 02.28	-69 38 03.5	Cluster-017	40650	23891456	N	
398	IRAS 05182-7117	05 17 34.61	-71 14 57.5	Cluster-016	40650	23891968	N	
441	MSX LMC 441	05 24 38.71	-70 23 56.8	MSX052438.7-702357	3505	12936448	Y	Z06
461	LHA 120-N 132E	05 24 19.30	-69 38 49.6	IRAS 05247-6941 ^h	1094	6076928	Y	
464	[HS66] 272	05 24 13.37	-68 29 58.9	HS 272	40159	22425088	N	
468	BSDL 1469	05 22 53.28	-69 51 10.4	Cluster-024	40650	23887872	N	
500	LI-LMC 861	05 21 29.69	-67 51 07.2	IRAS 05216-6753	1094	6076160	Y	
501	NGC 1936	05 22 12.55	-67 58 31.8	Cluster-006	40650	23882496	N	
560	IRAS 05300-6651	05 30 03.86	-66 49 24.2	05300-6651	200	6024704	Y	S08

Table 1—Continued

MSX LMC ^a	SIMBAD Name ^b	RA (J2000) ^c	Dec (J2000) ^c	Target Name ^d	PID ^e	AORKEY ^f	Public?	Ref. ^g
581	MSX LMC 581	05 26 46.63	-68 48 46.8	Cluster-002	40650	23884288	N	
596	IRAS 05311-6836	05 30 54.36	-68 34 27.8	Cluster-006	40650	23882496	N	
601	OGLE J052650.96-693136.8	05 26 50.83	-69 31 36.8	MSX052650.9-693136	3505	12935424	Y	Z06
635	IRAS 05278-6942	05 27 24.12	-69 39 45.0	MSX052724.3-693944	3505	12932864	Y	Z06
640	LHA 120-N 129	05 22 24.94	-69 42 32.4	Cluster-010	40650	23895040	N	
646	[MLD95] LMC 1-289	05 30 47.88	-71 07 55.2	LMC 1-289	30869	19150336	Y	
651	IRAS 05310-7110	05 30 20.16	-71 07 48.4	Cluster-042	40650	23894784	N	
690	MSX LMC 690	05 32 14.54	-71 13 28.2	Cluster-026	40650	23886848	N	
692	MSX LMC 692	05 28 46.63	-71 19 12.7	IRAS 05295-7121	3505	12929024	Y	Z06
733	IRAS 05348-7024	05 34 15.98	-70 22 52.7	05348-7024	200	6024448	Y	S08
766	LHA 120-N 150	05 33 42.22	-68 46 00.8	Cluster-014	40650	23892992	N	
771	MSX LMC 771	05 32 38.59	-68 25 22.1	MSX053238.7-682522	3505	12931328	Y	
805	LI-LMC 1163	05 32 35.62	-67 55 08.8	HV 996	200	6015744	Y	S08
811	MSX LMC 811	05 32 51.34	-67 06 51.8	05329-6708	200	6023168	Y	S08
886	IRAS 05389-6922	05 38 33.96	-69 20 31.6	IRAS 05389-6922	1094	6076416	Y	
887	IRAS 05406-6924	05 40 13.33	-69 22 46.5	HD 38489	30869	19149824	Y	
936	IRAS 05402-6956	05 39 44.86	-69 55 18.1	05402-6956	200	6020608	Y	S08
1117	IRAS 04498-6842	04 49 41.47	-68 37 51.2	IRAS 04498-6842	1094	6076672	Y	
1130	IRAS 04496-6958	04 49 18.50	-69 53 14.3	IRAS 04496-6958	1094	9069312	Y	S06
1171	IRAS 04545-7000	04 54 10.08	-69 55 58.4	04545-7000	200	6020352	Y	S08
1183	BSDL 126	04 51 53.66	-69 23 28.3	Cluster-003	40650	23883776	N	
1184	IRAS 04530-6916	04 52 45.67	-69 11 49.6	04530-6916	200	6023936	Y	S08
1190	IRAS 04516-6902	04 51 29.02	-68 57 49.7	04516-6902	200	6020096	Y	S08
1191	WOH S 60	04 53 30.86	-69 17 49.9	GV 60	40159	22402560	Y	
1192	IRAS 04509-6922	04 50 40.46	-69 17 31.9	04509-6922	200	6022400	Y	S08
1193	MSX LMC 1193	04 50 23.40	-69 37 56.6	IRAS04506-6942	30788	19009792	Y	
1207	LHA 12-N 89	04 55 06.58	-69 17 08.5	Cluster-022	40650	23888896	N	
1225	MSX LMC 1225	04 57 47.98	-66 28 44.8	Cluster-007	40650	23881984	N	

Table 1—Continued

MSX LMC ^a	SIMBAD Name ^b	RA (J2000) ^c	Dec (J2000) ^c	Target Name ^d	PID ^e	AORKEY ^f	Public?	Ref. ^g
1247	PGMW 3123	04 56 47.04	-66 24 31.3	lmc-hii-34	40159	22469632	Y	
1278	IRAS 05009-6616	05 01 04.42	-66 12 40.3	IRAS 05009-6616	3505	12929536	Y	Z06
1296	HD 32364	04 57 14.33	-68 26 30.5	HD 32364	30869	19150592	Y	
1302	IRAS 04589-6825	04 58 46.27	-68 20 42.7	IRAS04589-6825	30788	19010304	Y	
1438	HD 269997	05 41 21.19	-69 04 38.6	HD 269997	40159	22440704	N	
1453	IRAS 05506-7053	05 49 56.54	-70 53 11.8	IRAS05506-7053	30788	19005952	Y	
1651	MSX LMC 1651	06 02 45.10	-67 22 43.3	LI-LMC 1817 ^h	1094	6078208	Y	

^aMSX LMC identifier (EVP01).

^bObject name in SIMBAD (simbad.u-strasbg.fr/sim-fid.pl).

^cMSX LMC source position from SIMBAD

^dObject name as given in the headers of the data.

^eSpitzer program identifier.

^fUnique identifier for the astronomical observation request (AOR).

^gReferences. – S08: Sloan et al. 2008; S06: Speck et al. 2006; Z06: Zijlstra et al. 2006.

^hFor these objects, the target name does not match the position observed, possibly due to misidentification or pickup failure. In all cases, the position observed matches the position of the MSX LMC source.

All of the targets except MSX LMC 500 were observed with the low-resolution (SL and LL) modules of the IRS. They extend from 5.2 – 14 μm (SL) and 14 – 38 μm (LL), with resolving powers of 64 – 128. The SL module has a slit width of 3.6 – 3.7", and the LL module a slit width of 10.5 – 10.7". The raw data were processed through the *Spitzer* pipeline versions S15.3 or later. After pipeline processing, the basic calibrated data (BCDs) were cleaned for rogue pixels, using the IRSCLEAN software². For objects observed in staring mode (all except MSX LMC 1247), spectra were extracted using the SMART software³ (Higdon et al. 2004). Where multiple exposures were obtained, the two-dimensional spectral images (BCDs) of the multiple exposures were median-combined. Off-source regions of each spectral image served as sky background for the spectral image obtained with each module. Spectra were extracted and the fluxes were calibrated in SMART using the default point source extraction apertures. The modules at each nod position were merged and the edges and overlapping regions of the modules were trimmed. The spectra from the two nod positions were then averaged to produce the final spectrum. Uncertainty images are provided by the SSC pipeline and propagated through SMART to produce the uncertainties on the final spectra.

For 11 sources, a flux jump of $\gtrsim 5\%$ was observed between the SL and LL module spectra ($\sim 14 \mu\text{m}$). These were due to extended emission falling in the IRS slits and the differing widths of the SL and LL slits (see, e.g., Paper I). In most cases, the LL spectrum was scaled down to match the SL spectrum, but for the sources identified as H II regions the SL was scaled up to match the LL spectrum (§3).

One source, MSX LMC 1247, was observed in mapping mode. For each module and order (SL1, SL2, LL1, and LL2), a spectral cube was constructed using the Cubism software (Smith et al. 2007). Individual BCDs were background subtracted, using the corresponding off-source module, and corrected for bad pixels before the cubes were built. One-dimensional spectra were then extracted by integrating over a 10" region around the source in each cube.

MSX LMC 500 was observed with the SL module and both high resolution modules (SH and LH) of the IRS. The high resolution modules produce spectra covering 10 – 19 μm (SH) and 19 – 37 μm (LH), with a resolving power of ~ 600 . The reduction of the high resolution modules was carried out in the same manner as for the low resolution data, except for the background subtraction and the extraction aperture. No separate sky observations were taken for these data, so the sky background as a function of wavelength was estimated using SPOT and subtracted from the spectra after extraction. The high resolution spectra were extracted and fluxes calibrated using the default full extraction aperture in SMART. There are mismatches in flux between the orders in the LH spectrum which are most likely due to poor sky subtraction. These were rectified by scaling the longer wavelength order to match the shorter wavelength order. No such mismatches

²IRSCLEAN was written by the IRS GTO team (G. Sloan, D. Devost, & B. Sargent). It is distributed by the *Spitzer* Science Center at Caltech.

³SMART was developed by the IRS Team at Cornell University and is available through the *Spitzer* Science Center at Caltech.

are observed in the SH spectrum, though the SH spectrum was divided by a factor of 1.2 to match the SL spectrum.

3. SPECTRA AND CLASSIFICATIONS

In this section we present the previously unpublished spectra and classify them according to their spectral features. Table 2 lists the predicted JHK8 object classes from Paper II, the dominant spectral features and luminosity we determined from the IRS spectrum, and the ‘actual’ (most probable) object class based on the available information, for the 44 archival sample objects for which data are published or available (see §2 and Table 1). We note that, for the previously published spectra, our classifications agree with those of the publishing authors in all cases except two (MSX LMC 1190 and 1192; see §3.1.1), for which we adopt the classification of Sloan et al. (2008). Infrared (1 – 100 μm) luminosities were estimated from the IRS spectra and 2MASS photometry using the method outlined in Paper I. Typical uncertainties in the luminosity for the stellar sources are up to 15%, ignoring the effects of variability, but may be a factor of a few for the compact H II regions, where the bulk of the luminosity comes from wavelengths longer than the IRS spectral range. In the following subsections, we discuss the spectral classifications arranged according to object class.

Table 2. Summary of classifications

MSX LMC number	JHK8 ^a Class	Spectral ^b Features	Ref. ^c	Fig.	L _{IR} ($\times 10^4 L_{\odot}$)	Object ^b Class
283	-	O-RICH	S08	O AGB
1190	-	O-RICH	S08	O AGB
1192	GMV:	O-RICH	S08	O AGB
811	C AGB:	O-RICH ^d	S08	OH/IR
936	C AGB	O-RICH ^d	S08	OH/IR
1171	C AGB:	O-RICH ^d	S08	OH/IR
43	RSG	O-RICH	S08	RSG
461	RSG/GMV	O-RICH ^e	this paper	1	18:	RSG
805	RSG	O-RICH	S08	RSG
886	-	O-RICH	this paper	1	10	RSG
1117	RSG/GMV	O-RICH	this paper	1	11	RSG
1191	RSG	O-RICH ^f	this paper	1	7.0	RSG
500	H II	O-RICH ^f	this paper	1	16	RSG?
262	C/O AGB:	O-RICH	this paper	1	8.3	B[e]
323	-	O-RICH	this paper	1	1.7	B[e]
887	C/O AGB:	O-RICH	this paper	1	2.6	B[e]
134	-	PAH/O-RICH	this paper	1	11	B[e]?
44	C AGB	C-RICH	Z06	C AGB
47	C AGB:	C-RICH	Z06	C AGB
196	-	C-RICH	this paper	2	2.3	C AGB
219	H II:	C-RICH	Z06	C AGB
223	-	C-RICH	Z06	C AGB
307	C AGB:	C-RICH	Z06	C AGB
341	C AGB:	C-RICH	Z06	C AGB
349	-	C-RICH	Z06	C AGB
441	-	C-RICH	Z06	C AGB
560	C AGB	C-RICH	S08	C AGB
601	-	C-RICH	Z06	C AGB
635	-	C-RICH	Z06	C AGB
692	C AGB	C-RICH	Z06	C AGB
733	C AGB:	C-RICH	S08	C AGB
1130	C/O AGB	C-RICH	S06	C AGB
1278	C AGB:	C-RICH	Z06	C AGB

Table 2—Continued

MSX LMC number	JHK8 ^a Class	Spectral ^b Features	Ref. ^c	Fig.	L _{IR} ($\times 10^4 L_{\odot}$)	Object ^b Class
1302	H II?	C-RICH?	this paper	2	0.2:	C AGB?
1453	C AGB:	C-RICH	this paper	2	1.7	C AGB
1651	C AGB:	C-RICH	this paper	2	1.2	C AGB
198	H II	PAH	this paper	3	2.6	H II
646	H II:	PAH	this paper	3	1.7	H II
1247	H II	PAH	this paper	3	10	H II
1296	H II	PAH	this paper	3	5.4	H II
46	-	PAH	this paper	4	1.6	YSO?
771	C AGB	PAH?	this paper	4	2.5	YSO?
1184	C AGB	PAH	S08	YSO
1193 ^g	C AGB	

^aPaper II color-color classification.

^bSpectral features refers to the dominant dust features in the IRS spectrum which are usually unambiguous. The object class refers to our classification of the object, based on its spectral features and other information, which is somewhat more uncertain.

^cS08: Sloan et al. 2008; S06: Speck et al. 2006; Z06: Zijlstra et al. 2006.

^dThese objects show silicate self-absorption.

^eThe LL spectrum is contaminated by emission from a nearby source blended with that of MSX LMC 461. See text for details.

^fSurrounded by H II region.

^gThis object was not detected due to mispointing.

3.1. Oxygen-rich objects

We group the classes of object that have oxygen-rich dust chemistry together, and discuss them in the following subsections. Seventeen objects were identified as having oxygen-rich chemistry from their IRS spectra. Figure 1 shows the 9 spectra that have not previously been published. Stars with oxygen-rich circumstellar dust show broad silicate features at 9.7 and 18 μm , usually in emission. While oxygen-rich circumstellar dust is easy to identify on the basis of its mid-IR spectral features, classifying the nature of a visually obscured star with an O-rich circumstellar envelope as an AGB star or a red supergiant requires an assessment of its bolometric luminosity. The O-rich objects in this sample include 3 O-rich AGB stars, 3 OH/IR stars, 7 red supergiants (RSGs), one of which is a tentative classification, and 4 dusty, early-type stars. We now discuss each of these subcategories describing individual objects and spectra where appropriate.

3.1.1. O-rich asymptotic giant branch stars

Three of the O-rich stars listed in Table 2, MSX LMC 283, 1190, and 1192, were classified as AGB stars by Sloan et al. (2008). MSX LMC 283 has an IR luminosity $1.4 \times 10^4 L_{\odot}$, and is clearly an AGB star. MSX LMC 1190 and 1192 both have IR luminosities $\sim 7 \times 10^4 L_{\odot}$, just above the classical limit for AGB stars, suggesting they are RSGs; however, we adopt the classification of Sloan et al. (2008), who class these two stars as O-rich AGB stars on the basis of their amplitudes of K-band variability.

3.1.2. OH/IR stars

Three oxygen-rich sources show silicate self-absorption at 9.7 μm . All three, MSX LMC 811, 936, and 1171, are classified as OH/IR stars — i.e., O-rich AGB stars with especially optically thick circumstellar envelopes and that display OH maser emission — by Sloan et al. (2008).

3.1.3. Red supergiants

Seven objects were classified as red supergiants (RSGs) on the basis of their *Spitzer* spectral features and luminosity. These objects all have estimated luminosities $\gtrsim 7.0 \times 10^4 L_{\odot}$.

MSX LMC 43 and *MSX LMC 805*: These stars are classified as RSGs by Sloan et al. (2008).

MSX LMC 461: The rising SED of RSG MSX LMC 461 above $\sim 20 \mu\text{m}$ is likely due to a contaminating source in the LL module slits. The 24 μm SAGE image shows that MSX LMC 461 is in a cluster at the center of an H II region, with 3 bright 24 μm sources within $\sim 25''$. The nearest of these is separated by $11''$ according to the SAGE 24 μm catalog. The 24 μm flux of the contaminating source is 347 mJy, making it slightly brighter than MSX LMC 461 (335 mJy), but it does

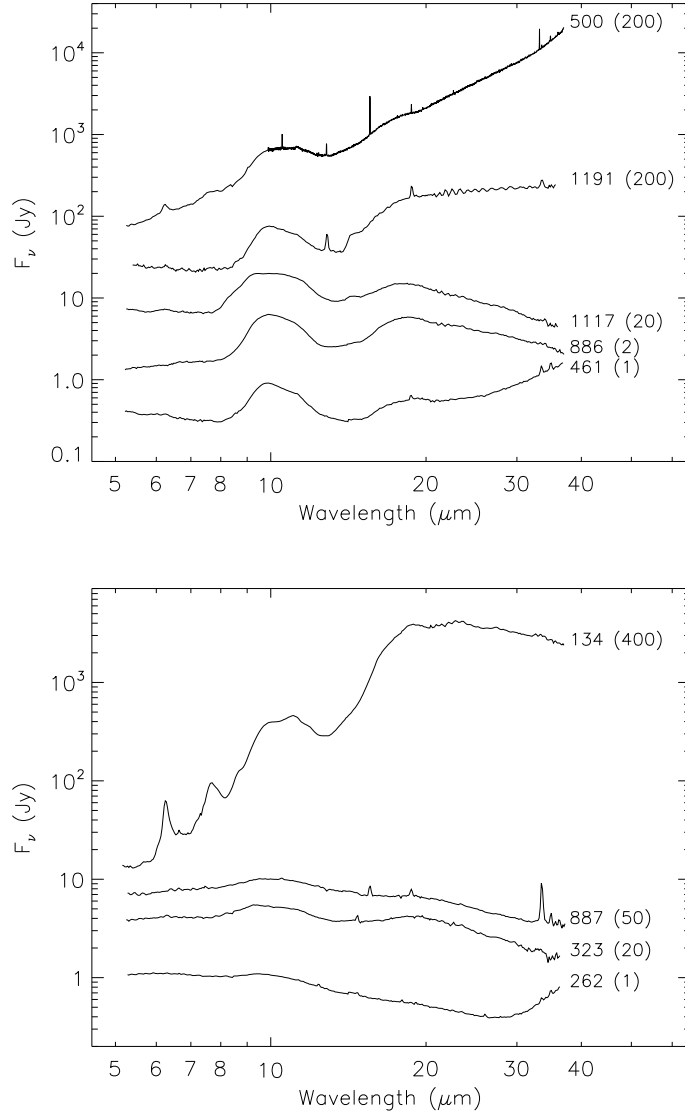


Fig. 1.— IRS spectra of objects spectroscopically identified as oxygen-rich. *Top panel:* Red supergiants. *Bottom panel:* Known and candidate B[e] stars. The MSX LMC number of each source is listed by the spectrum and, for clarity, spectra are multiplied by the factor indicated in parentheses. Where a flux disparity occurs between the SL and LL modules (see text) the LL module has been scaled to the SL module flux.

not appear in the IRAC catalog or images, indicating it is very red. An overlay of the observed slit positions on the 24 μm image indicates this source fell in the LL slits. Examination of the LL1 and LL2 spectral images reveals that two blended sources separated by ~ 2 pixels ($5.1''/\text{pixel}$) can be distinguished at the shorter wavelengths ($\lesssim 27 \mu\text{m}$). As these sources are heavily blended, no attempt was made to separate their spectra. In addition, the SAGE 70 μm image shows diffuse emission due to cold dust in the surrounding H II region, which may also have contaminated the longer wavelengths of the IRS spectrum. Therefore, the luminosity for MSX LMC 461 was estimated using only the SL module spectra (5.2 – 14 μm). While the luminosity is therefore somewhat uncertain, it is still sufficiently high ($1.8 \times 10^5 L_{\odot}$) to confidently classify it as an RSG. The LL spectrum was scaled by 0.94 to match the SL spectrum.

MSX LMC 886: Although the JHK8 colors and magnitudes of MSX LMC 886 are more similar to O-rich AGB stars than RSGs, we estimate its IR luminosity to be $10^5 L_{\odot}$, and Wood et al. (1992) identify it as a probable core He-burning supergiant as it shows no large-amplitude variability.

MSX LMC 1117: This star has a luminosity of $1.1 \times 10^5 L_{\odot}$, placing it clearly in the RSG category.

MSX LMC 1191: We classify this star as a RSG due to its luminosity of $7 \times 10^4 L_{\odot}$. This unusual spectrum, with a flat mid-IR slope, is reminiscent of sources with dust disks (see Kastner et al. 2006) and, since these are of special interest, MSX LMC 1191 warrants further investigation. No contaminating source is readily apparent in the spectral image of MSX LMC 1191. This object appears point-like in the SAGE 24 μm image, although there is faint [Ne II] 12.8 μm , [S III] 18.7 μm , and [S III] 33.5 μm emission off-source and a small SL/LL jump suggests extended emission is associated with the source. The LL spectrum was scaled by 0.90 to match the SL spectrum.

MSX LMC 500: This star appears to be a mass-losing O-rich evolved star within an H II region. The spectrum clearly shows silicate features in emission, but also has a rising continuum, and features typical of H II regions, including PAH features at 6.2 μm , 7.7 μm , and 11.2 μm , and emission lines [S IV] 10.5 μm , [Ne II] 12.8 μm , [Ne III] 15.5 μm , [S III] 18.7 μm , [S III] 33.5 μm , [Si II] 34.8 μm , and [Ne III] 36.0 μm . Although it is not included in the SAGE 24 micron point source catalog, SAGE IRAC and MIPS images show a bright point source surrounded by strong nebulosity at the position of MSX LMC 500. The contamination of this spectrum by the H II region prevents certain identification of this object as an O-rich evolved star as opposed to a massive YSO, but here we tentatively classify it as a RSG (rather than an O-rich AGB star), on the basis of its high luminosity ($1.6 \times 10^5 L_{\odot}$). We note that this classification is uncertain, as the luminosity includes a significant contribution from the contaminating H II region.

3.1.4. *Dusty, early-type stars*

Three of the objects showing O-rich dust are known B[e] supergiants (Paper II). These three, MSX LMC 262, 323, and 887, all show flat IRS spectra with (relatively weak) silicate features in emission (Figure 1). In addition, the source MSX LMC 134 – which displays perhaps the most peculiar spectrum among the IR sources considered here – is associated with a luminous O/B star. These four sources will be discussed in more detail in a forthcoming paper on *Spitzer* observations

of dusty early-type stars in the Magellanic Clouds (J. Kastner et al. 2009, in preparation).

MSX LMC 262: The spectrum of this star (HD 34664) has slowly falling (blue) continuum and what appears to be weak silicate features. This source is affected by contamination from diffuse line emission, as is apparent in the spectral images, although this appears to be effectively removed by the sky subtraction. The rising continuum above $\sim 29 \mu\text{m}$ is attributable to a nearby contaminating source, observed in IRAC and MIPS images, which is very red and blended with MSX LMC 262. The LL spectrum was scaled by 0.96 to match the SL spectrum.

MSX LMC 323: MSX LMC 323 (LHA 120-S 93) shows the strongest silicate emission features among the 3 B[e] supergiants with spectra in Figure 1. There is a small jump in flux density between the SL and LL modules, consistent with faint diffuse emission in the LL module spectral images; however no narrow emission lines are observed in the sky or the stellar spectrum. The LL spectrum was scaled by 0.85 to match the SL spectrum.

MSX LMC 887: In addition to the broad silicate features, this star (HD 38489) shows narrow emission lines that we identify as [Ne III] $15.5 \mu\text{m}$ and [S III] $18.7 \mu\text{m}$. Examination of the spectral images indicates that these lines arise from extended, diffuse emission and not from the star itself. Also present in the images are emission lines of [S IV] $10.5 \mu\text{m}$, [Ne II] $12.8 \mu\text{m}$, [S III] $33.5 \mu\text{m}$, and [Si II] $34.8 \mu\text{m}$, which are too weak to show up in the extracted stellar spectrum. The spectrum of MSX LMC 887 also shows a large jump in flux density (a factor of ~ 5) between the SL and LL modules, most likely due to extended emission apparent in the LL module spectral images. The LL spectrum was scaled by 0.21 to match the SL spectrum. SAGE $8 \mu\text{m}$ and $24 \mu\text{m}$ images show this star to be a point source surrounded by nebulous emission associated with a H II region, consistent with the presence of the ionized gas seen in the spectral images.

MSX LMC 134: This star (HD 269006) shows a peculiar spectrum with very strong silicate emission feature, strong PAH emission at $6.2 \mu\text{m}$ and $7.7 \mu\text{m}$, and a steeply rising continuum that flattens above $\sim 20 \mu\text{m}$. This flattened spectral shape is suggestive of a dust disk with a large central hole or gap.

3.2. Carbon-rich AGB stars

Nineteen of the objects in the archival sample are classified as carbon-rich on the basis of their *Spitzer* IRS spectra. They are characterized by an absorption feature at $8 \mu\text{m}$ due to C_2H_2 and HCN, a SiC dust emission feature at $11.3 \mu\text{m}$, a narrow absorption feature at $13.7 \mu\text{m}$ due to C_2H_2 gas, and a broad emission feature around $26 - 30 \mu\text{m}$ attributed to MgS (Goebel & Moseley 1985; Hony et al. 2002). Figure 2 shows the IRS spectra of the 4 objects for which IRS data have not previously been published (see Tables 1 and 2). The references for the remaining 15 are listed in Table 2. The LL spectrum of MSX LMC 1651 was scaled by 0.91 to match the SL spectrum.

The classification of MSX LMC 1302 is somewhat uncertain, due to the relatively low signal-to-noise of the spectrum and the presence of a large (factor ~ 5) jump between the SL and LL

modules. The LL spectrum was scaled by a factor 0.19 to match the SL spectrum. This jump is most likely due to diffuse extended emission that is due to cool dust, as seen in the SAGE 8.0 μm and 24 μm images as well as in the LL spectral images. The LL images also reveal [S III] 33.5 μm and [Si II] 34.8 μm emission surrounding the source, but this emission is too weak to be apparent in the spectrum.

3.3. Compact H II regions

Figure 3 shows the spectra of the 4 objects identified as compact H II regions or candidate compact H II regions on the basis of their IRS spectra. These sources are characterized by very red continua, strong PAH emission features at 6.2, 7.7, 8.6, 11.3, and 12.7 μm , silicate absorption at 9.7 μm , and the following lines of ionized species: [Ar III] 9.0 μm , [S IV] 10.5 μm , [Ne II] 12.8 μm , [Ne III] 15.5 μm , [S III] 18.7 μm , [S III] 33.5 μm , [Si II] 34.8 μm , and [Ne III] 36.0 μm . All these sources except MSX LMC 1247 also show a flux difference at 14 μm between the SL and LL modules, due to their extended nature; in Figure 3, the SL spectra have been scaled by factors 1.4 – 2.6 to match the LL fluxes. No flux jump is seen in MSX LMC 1247 as it was observed in mapping mode.

3.4. Young Stellar Objects and Candidates

One star in the sample, MSX LMC 1184, has been classified as a young stellar object (YSO) based on its optical and IR properties (Sloan et al. 2008). It shows a red continuum, similar to H II regions, with PAH emission and silicate absorption features, but lacks the narrow ionized line emission observed in H II regions. We find two more objects in the sample with somewhat similar IR spectra, and group them here with 1184, though we note their classification as candidate YSOs is very tentative.

MSX LMC 46: The spectrum of this star resembles the spectrum of YSO MSX LMC 1184 presented by Sloan et al. (2008), and shows much weaker line emission and PAH features than the H II regions, which have similar red continua (Figure 4). The LL spectrum was scaled by 0.74 to match the SL spectrum. Figure 5 shows the SL spectrum of MSX LMC 46, with a spline-fitted continuum subtracted to highlight the PAH features and silicate absorption. It is possible this object is a high-mass protostar in transition from the embedded young stellar object (YSO) stage to the zero-age main sequence.

MSX LMC 771: MSX LMC 771 shows a similar continuum shape to MSX LMC 1184 (Figure 4), but the nature of this source is uncertain. The only clear spectral feature in this spectrum is silicate absorption at 9.7 μm . The silicate absorption profile is more sharply peaked, and the PAH features are significantly weaker than in MSX LMC 1184 and 46. This source may be a compact H II region, though it lacks the lines of ionized species normally observed in the spectra of H II regions. Weak emission lines [Ne III] 15.5 μm , [S III] 18.7 μm , [S III] 33.5 μm , and [Si II] 34.8 μm , and lines at 16.4 μm and 17.1 μm , are apparent in the spectral images, but do not appear in the extracted

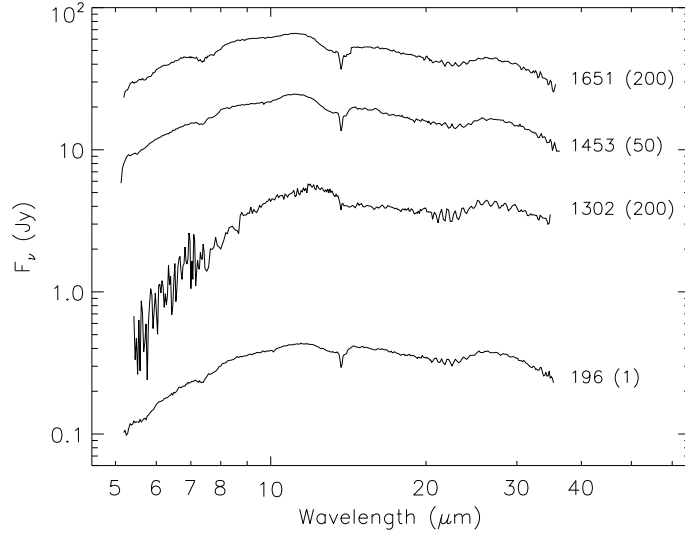


Fig. 2.— IRS spectra of objects identified as C-rich AGB stars. The MSXLMC number of each source is listed by the spectrum and, for clarity, spectra are multiplied by the factor indicated in parentheses. Where a flux disparity occurs between the SL and LL modules (see text) the LL module has been scaled to the SL module flux.

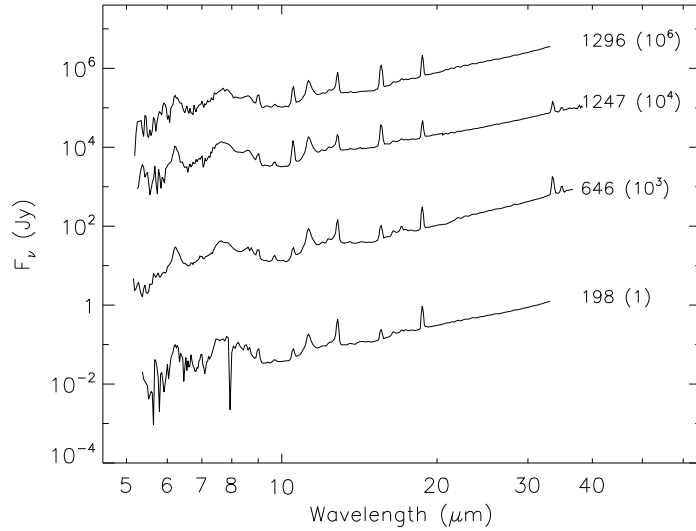


Fig. 3.— IRS spectra of objects identified as H II regions. The MSXLMC number of each source is listed by the spectrum and, for clarity, spectra are multiplied by the factor indicated in parentheses. Where a flux jump occurs between the SL and LL modules, the SL spectrum was scaled to match the LL spectrum (see text).

spectrum. SAGE 8 and 24 μm images show this object to be a bright point source located within a nebulous region. It is possible this source is an embedded YSO. The LL spectrum was scaled by 0.94 to match the SL spectrum.

MSX LMC 1184: This star has been identified as a young stellar object (YSO; Sloan et al. 2008; van Loon et al. 2005), based on its optical and IR spectral features and its IR colors. This source shows a red continuum, with PAH emission features and silicate absorption at 9.7 μm .

3.5. Unclassified sources

The observation of MSX LMC 1193 was mispointed; therefore this object was not detected and could not be classified.

4. CHECKING AND IMPROVING THE JHK8 CLASSIFICATIONS

We now compare the spectral classifications described in §3 with the classifications of the same sources based on JHK8 scheme (Paper II). Where the JHK8 prediction (column 2 of Table 2) matches the actual classification (column 7), the prediction is considered correct. JHK8 classifications are considered incorrect where column 2 does not match column 7. For these purposes, uncertain JHK8 predictions (indicated by a colon in column 2) are considered the same as firm predictions. Where the JHK8 class was ambiguous due to overlaps in the classification boxes (e.g., RSG/GMV), we consider the prediction to be “correct but ambiguous” if one of the two classes in column 2 matches the classification in column 7. Objects for which no JHK8 classification was possible (due to their location outside the boxes in color-color plots) are considered neither correct nor incorrect. Figure 6 shows the locations and JHK8 classifications of the 44 objects with published or available archival spectra in the 2MASS/MSX color-color diagrams, along with the JHK8 diagnostic regions used previously to classify the object classes (Paper II). Figure 7 shows the IRS-based spectral classifications of the archival objects in the 2MASS/MSX color-color diagrams. 2MASS/MSX magnitudes of all sources are given in Paper II.

In summary, of the sample of 44 objects, the JHK8 scheme correctly predicted the classification for 17 sources, and a further 5 had correct but ambiguous classifications, where we have included C/O AGB as an ambiguous match for the dusty early-type stars. Nine sources had incorrect classifications. Twelve objects had no JHK8 classification and, as noted earlier, one source could not be classified on the basis of its IRS spectrum.

In the following subsections we discuss the JHK8 classifications of each object class in more detail. We combine the new IRS-based classification results with those obtained in Paper I so as to revise and expand the JHK8 classification boxes. The color-color diagrams of the whole sample of 250 objects are shown in Figure 8, with the expanded classification boxes. The revised classification criteria are listed in Table 3.

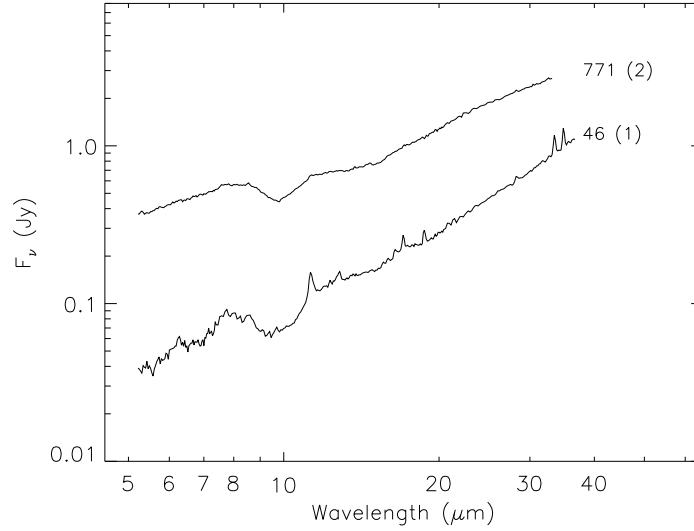


Fig. 4.— IRS spectra of candidate young stellar objects. The MSX LMC number of each source is listed by the spectrum and, for clarity, spectra are multiplied by the factor indicated in parentheses. The LL spectra were scaled to match the SL spectra (see text).

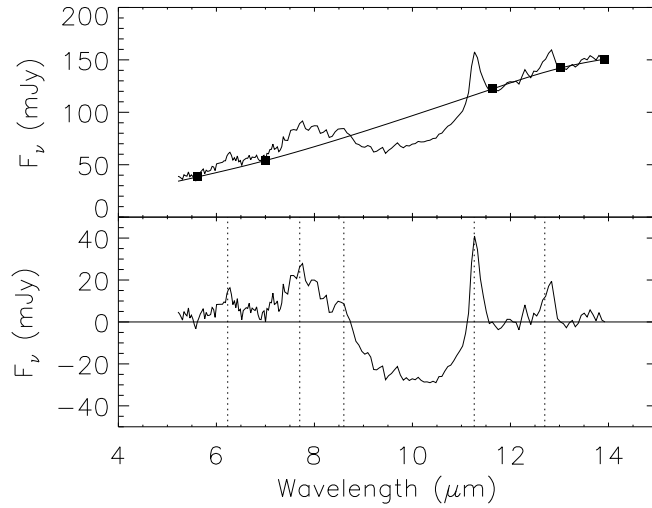


Fig. 5.— SL module spectrum of MSX LMC 46. *Top panel:* the spline (*thin line*) fitted to the continuum points (*squares*). *Bottom:* The spline-subtracted spectrum, highlighting the PAH emission features at wavelengths 6.23, 7.70, 8.60, 11.26, and 12.70 μm (*dotted lines*).

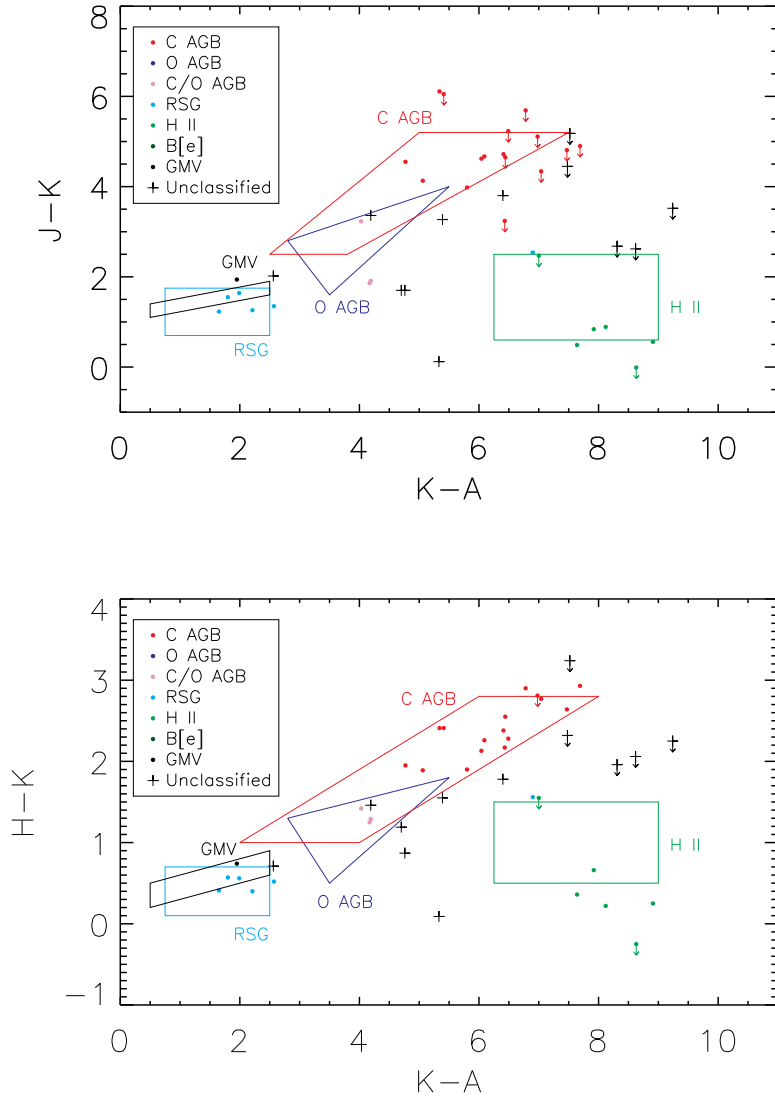


Fig. 6.— JHK8 classifications of the available *Spitzer* archival sources in the 2MASS/MSX color-color diagrams. Symbols indicate the JHK8 classification of each object from Paper II. Arrows indicate limits. The enclosed areas represent the classification regions defined in Paper II.

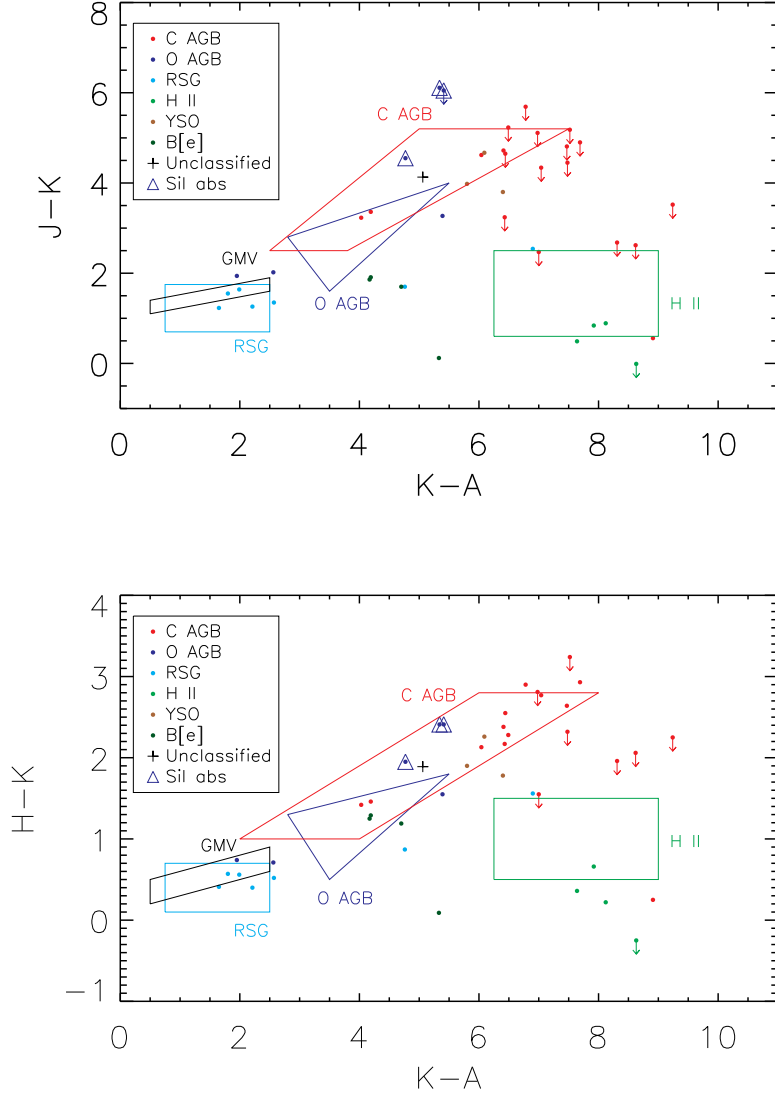


Fig. 7.— 2MASS/MSX color-color diagrams for the sources with confirmed spectroscopic classifications from archival *Spitzer* data. Colors indicate the class of each object (Table 2). Arrows indicate limits and boxes indicate the JHK8 classification regions from Paper II. The three sources with silicate self-absorption, which have been classified as OH/IR stars by Sloan et al. (2008), are enclosed by triangles (see §4.1.2).

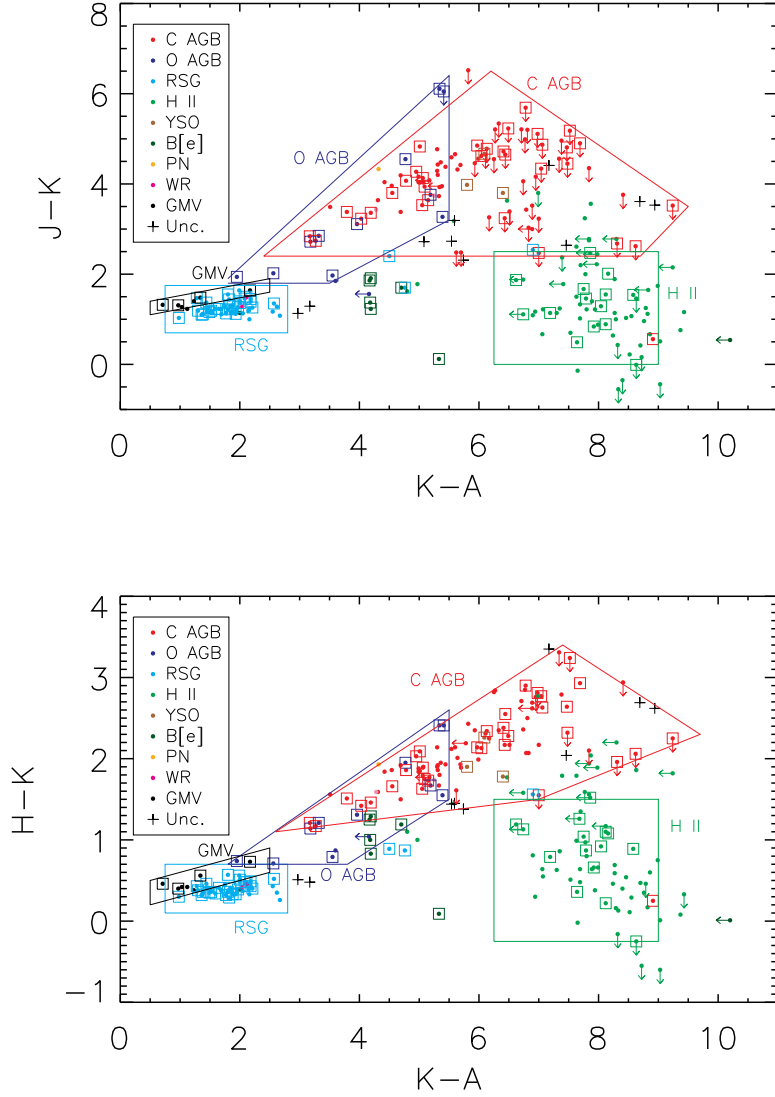


Fig. 8.— 2MASS/MSX color-color diagrams for the whole sample of the 250 brightest $8 \mu\text{m}$ sources in the LMC (Paper II). Colors indicate the class of each object (from Paper II and Table 2) and plus signs show objects which are unclassified. Arrows indicate limits. Open squares indicate objects whose classification is spectroscopically verified with IRS spectra. Boxes indicate the revised JHK8 classification regions.

Table 3. Luminous LMC Mid-IR Sources: Revised JHK8 Color Classification Criteria

Class	Criteria	
J-K vs. K-A colors		
RSG	$0.75 \leq (K-A) \leq 2.7$	$0.7 \leq (J-K) \leq 1.75$
O AGB	$2.0 \leq (J-K); (K-A) \leq 5.5$	$[0.7 \times (K-A) - 0.65] \leq (J-K) \leq [1.24 \times (K-A) - 0.42]$
C AGB	$[0.93 \times (J-K) + 0.16] \leq (K-A) \leq [0.73 \times (J-K) + 6.95]$	$2.4 \leq (J-K) \leq [-0.91 \times (K-A) + 12.15]$
H II	$6.25 \leq (K-A) \leq 9.0$	$0.0 \leq (J-K) \leq 2.5$
Expanded H II	$6.0 \leq (K-A) \leq 9.5$	$(J-K) \leq 3.0$
GMV	$0.5 \leq (K-A) \leq 2.5$	$[0.25 \times (K-A) + 0.975] \leq (J-K) \leq [0.25 \times (K-A) + 1.275]$
H-K vs. K-A colors		
RSG	$0.75 \leq (K-A) \leq 2.7$	$0.1 \leq (H-K) \leq 0.7$
O AGB	$0.7 \leq (H-K); (K-A) \leq 5.5$	$[0.47 \times (K-A) - 1.09] \leq (H-K) \leq [0.51 \times (K-A) - 0.21]$
C AGB	$[2.08 \times (H-K) + 0.31] \leq (K-A) \leq [3.33 \times (H-K) + 2.0]$	$[0.09 \times (K-A) + 0.86] \leq (H-K) \leq [-0.48 \times (K-A) + 6.94]$
H II	$6.25 \leq (K-A) \leq 9.0$	$-0.25 \leq (H-K) \leq 1.5$
Expanded H II	$6.0 \leq (K-A) \leq 9.5$	$(H-K) \leq 2.0$
GMV	$0.5 \leq (K-A) \leq 2.5$	$[0.2 \times (K-A) + 0.1] \leq (H-K) \leq [0.2 \times (K-A) + 0.4]$

Table 4. Luminous LMC Mid-IR Sources: Revised IRAC/MIPS Color Classification Criteria

Class	Criteria
	[3.6]–[4.5] vs. [5.8]–[8.0] colors
RSG	$[-1.00 \times ([3.6] - [4.5]) + 0.20] \leq [5.8] - [8.0] \leq [-1.00 \times ([3.6] - [4.5]) + 1.00]$ $[1.29 \times ([5.8] - [8.0]) - 0.95] \leq [3.6] - [4.5] \leq [1.29 \times ([5.8] - [8.0]) - 0.37]$
O AGB	$[-1.00 \times ([3.6] - [4.5]) + 1.40] \leq [5.8] - [8.0] \leq [-1.25 \times ([3.6] - [4.5]) + 2.06]$ $[9.00 \times ([5.8] - [8.0]) - 10.6] \leq [3.6] - [4.5] \leq [1.25 \times ([5.8] - [8.0]) - 0.40]$
C AGB	$[-0.50 \times ([3.6] - [4.5]) + 0.73] \leq [5.8] - [8.0] \leq [-0.43 \times ([3.6] - [4.5]) + 2.14]$ $[1.39 \times ([5.8] - [8.0]) - 0.42] \leq [3.6] - [4.5] \leq [1.44 \times ([5.8] - [8.0]) - 0.08]$
	[5.8]–[8.0] vs. [8.0]–[24] colors
RSG	$[-2.12 \times ([5.8] - [8.0]) + 2.33] \leq [8.0] - [24] \leq [-2.67 \times ([5.8] - [8.0]) + 4.59]$ $[0.38 \times ([8.0] - [24]) - 0.43] \leq [5.8] - [8.0] \leq [0.55 \times ([8.0] - [24]) - 0.18]$
O AGB	$[-5.94 \times ([5.8] - [8.0]) + 8.15] \leq [8.0] - [24] \leq [-1.11 \times ([5.8] - [8.0]) + 4.14]$ $[5.8] - [8.0] \leq [0.53 \times ([8.0] - [24]) - 0.13]$
C AGB	$0.42 \leq ([5.8] - [8.0]) ; [8.0] - [24] \leq [-0.45 \times ([5.8] - [8.0]) + 3.04]$ $[0.56 \times ([8.0] - [24]) - 0.20] \leq [5.8] - [8.0] \leq [0.41 \times ([8.0] - [24]) + 0.44]$
	J–K vs. [3.6]–[4.5] colors
RSG	$[-0.08 \times (J - K) - 0.09] \leq [3.6] - [4.5] \leq [-0.06 \times (J - K) + 0.41]$ $[0.40 \times ([3.6] - [4.5]) + 0.86] \leq J - K \leq [0.39 \times ([3.6] - [4.5]) + 1.68]$
O AGB	$[0.10 \times (J - K) - 0.05] \leq [3.6] - [4.5] \leq [0.15 \times (J - K) + 0.17]$ $1.9 \leq J - K \leq 6.2$
C AGB	$[0.50 \times (J - K)] \leq [3.6] - [4.5] \leq [0.18 \times (J - K) - 0.05]$ $[-0.75 \times ([3.6] - [4.5]) + 3.02] \leq J - K \leq [4.27 \times ([3.6] - [4.5]) + 12.54]$

4.1. Oxygen-rich objects

Of the 17 objects with O-rich dust chemistry, 12 had JHK8 classifications (Table 2). Of these, 3 classifications were correct and a further 4 were ambiguously correct, while 5 were incorrect. The classes of O-rich object are discussed in the following subsections.

4.1.1. *O-rich asymptotic giant branch stars*

Of the three sources classified as O-rich AGB stars on the basis of IRS spectra (Table 2), MSX LMC 1192 had a tentative JHK8 classification of GMV, while MSX LMC 283 and 1190 were previously unclassified by the JHK8 scheme. Thus none of these three sources lies in the previous (Paper II) O AGB classification box.

The IR colors of MSX LMC 283 (see Table 1 of Paper II) place it redward (in K-A) of the ambiguous overlap region of the O-rich and C-rich AGB stars. On the basis of the location of MSX LMC 283, we extend the O AGB box to the right in K-A (Figure 8). As the overlap area between O-rich and C-rich AGB stars now covers a large fraction of the region occupied by O-rich AGB stars, the classification of the majority of the O-rich AGB stars in a IR-luminous stellar population solely on the basis of their JHK8 colors will be ambiguous. However, the increased overlap is largely due to the location of the OH/IR stars (§4.1.2) and many of the O-rich AGB stars lie outside the overlap region. In addition, as discussed in Paper II, the O-rich and C-rich stars seem to be well-distinguished by their [8]-[24] μm SAGE colors (see §4.5).

MSX LMC 1190 and 1192 lie near the RSG classification box in the JHK8 scheme, bluer in K-A than the O-rich AGB box by ~ 1 mag. On the basis of the colors of MSX LMC 1190 and 1192, we extend the O AGB box to bluer K-A, covering the region between the previous O-rich AGB star and RSG classification boxes, and leading to a small overlap between the O AGB and GMV boxes. For objects in this region, additional information, such as the K magnitude, is necessary to determine the nature of the object.

4.1.2. *OH/IR stars*

The three OH/IR stars, MSX LMC 811, 936, and 1171, were all incorrectly classified by the JHK8 scheme as carbon-rich AGB stars. These stars show silicate self-absorption indicative of optically-thick dust shells due to high mass-loss rates. Their locations in the color-color diagrams (Figure 7) are indicative of increasingly strong self-absorption due to high mass-loss rates.

These objects lie above most carbon stars in the 2MASS/MSX color-color diagrams (i.e., for a given K-A color, the three OH/IR stars are generally redder in J-K and H-K than carbon stars) but are nevertheless within or above the JHK8 diagnostic box for C-rich AGB stars, suggesting

that for modestly self-absorbed objects, spectroscopy or additional photometry may be necessary to distinguish OH/IR stars from carbon stars. The O-rich AGB classification box has been expanded to include these objects, increasing the ambiguous overlap region between carbon-rich and oxygen-rich objects (Fig. 8).

4.1.3. *Red Supergiants*

Of the 7 RSGs, three were correctly classified as RSGs on the basis of JHK8 colors and two (MSX LMC 461 and 1117) had correct but ambiguous classifications of RSG/GMV. One object, MSX LMC 500, was incorrectly classified as an H II region and one object, MSX LMC 886, was not classifiable via JHK8 colors.

MSX LMC 500 was most likely misclassified due to the surrounding nebulous dust emission contaminating the JHK8 colors (see §3.1.3), as it lies close to the H II region classification box, ~ 5 magnitudes redder in K-A than typical RSGs. MSX LMC 886 lies ~ 2 magnitudes redder in K-A than typical RSGs, quite close to the O-rich AGB classification box. The Paper II RSG classification box covers the region of color-color space occupied by most of the RSGs and was not expanded or altered on the basis of the position of MSX LMC 500 or 886.

4.1.4. *Dusty, early-type stars*

Of the four dusty, early-type stars, two had correct but ambiguous JHK8 classifications, and two were unclassifiable via the JHK8 scheme. The former two, MSX LMC 262 and 887, lie within the O-rich AGB and C-rich AGB classification boxes in H-K vs. K-A but not J-K vs K-A (Fig. 8). The latter two objects, MSX LMC 323 and 134, have similar colors to 262 and 887 but lie outside the classification boxes. No dusty, early-type star classification box is defined, due to the small number of objects.

4.2. Carbon-rich AGB stars

Of the 19 C-rich sources, 10 were correctly classified as carbon-rich on the basis of their JHK8 colors, and one (MSX LMC 1130) was correctly but ambiguously classified as either C- or O-rich. Six objects lay outside the classification boxes in Figure 6 and so had no JHK8 classification, while two sources (MSX LMC 219 and 1302) were incorrectly classified as H II regions on the basis of their JHK8 colors.

The 6 C-rich AGB stars which could not be classified under the JHK8 system lie near the C-rich AGB diagnostic box (Figure 7) but have redder JKH8 colors. This region of color space was not covered by our Paper I observations but, on the basis of the new spectral data, we may now extend

the C-rich AGB star classification region to include objects with $K-A \gtrsim 6.5$, $J-K \gtrsim 2.5$, and $H-K \gtrsim 1.5$. The revised C AGB box covers the space between the Paper II C AGB box and the H II region classification box and results in a small overlap between the boxes (Figure 8). For objects with colors in the overlap region, imaging aimed at distinguishing between diffuse vs. point-like emission would be essential in the absence of spectroscopy to determine unambiguous classifications.

One of the two C-rich AGB stars which was incorrectly classified as an H II region (MSX LMX 219) lies in the overlap region between the C AGB and H II region boxes. The other star, MSX LMC 1302, lies well within the H II region classification box and away from the other C-rich AGB stars. The C AGB box was not extended to include 1302, due to the uncertainty of its classification and, in particular, the possibility that it may be a pre-planetary nebula.

4.3. Compact H II regions

For the four confidently classified H II regions, the JHK8 color scheme correctly predicted the spectral classification. The location of these objects expands the H II region classification box to bluer J-K and H-K colors (Fig. 8).

4.4. Young Stellar Objects and Candidates

Of the three YSO or YSO candidates in the sample, two were incorrectly classified as C-rich AGB stars by the JHK8 scheme and the other had no JHK8 classification. Although they resemble H II regions in their mid-IR spectra, MSX LMC 46, 771, and 1184 have redder J-K and H-K colors than H II regions. All three objects lie near each other and within the revised C AGB classification box. No YSO classification box is defined due to the small number of objects and the uncertain nature of their classifications.

4.5. *Spitzer* IRAC/MIPS classification of IR-luminous point sources

Figure 10 shows *Spitzer* IRAC/MIPS color-color diagrams for the sources in the whole sample of 250 objects with SAGE counterparts (see Paper II). Diagnostic regions defined by the spectroscopically classified objects are shown in Figure 10 and the corresponding IRAC/MIPS classification criteria for luminous IR sources, revised according to the IRS spectral classification results reported here, are listed in Table 4. As noted in Paper II, *Spitzer* IRAC and IRAC/MIPS color-color diagrams such as those in Fig. 9 provide better discrimination between carbon-rich and oxygen-rich AGB stars than do JHK8 color-color diagrams. This discrimination has been further improved by the IRS spectral classifications, which resulted in the reclassification of several apparent C-rich AGB stars as OH/IR stars (Table 2). Figure 10 shows the *Spitzer* IRAC [3.6]-[4.5] color plotted

against 2MASS J-K. While this diagram shows somewhat more overlap between the C-rich and O-rich AGB stars than do the *Spitzer* IRAC and IRAC/MIPS diagrams (Fig. 9), the J-K vs. [3.6]-[4.5] diagram will remain useful even after Spitzer enters its warm mission, in which only the 3.6 and 4.5 μm channels will operate. We note that the outlying C-rich AGB star in the bottom right corner of the diagram (MSX LMC 1302) is excluded from the ‘C AGB’ region as its colors may be affected by extended emission. Finally, we note that the two O-rich sources with J-K \sim 6 in this diagram are OH/IR stars that show silicate self-absorption.

5. SUMMARY AND CONCLUSIONS

We have used archival and published IRS spectra to classify 43 IR-luminous sources in the LMC. Of the 31 objects of these 43 that have a previous (Paper II) JHK8 classification, we find that the JHK8 classifications were correct for 22 objects (71%). Of the nine objects with incorrect JHK8 classifications, four had tentative classifications.

Spectroscopic classifications of the 12 objects which were previously unclassifiable with the JHK8 diagnostics allow us to characterize new regions of the 2MASS/MSX color-color diagrams. In addition, analysis of the IRS spectra obtained for the 9 objects which were previously incorrectly classified under the JHK8 scheme allows us to revise the classification boxes so as to make JHK8 color-based classifications more reliable. The area of color space occupied by C-rich AGB stars is extended to redder K-A colors, towards the location of H II regions. Similarly — as a consequence of the reclassification of 3 objects from C-rich AGB (Paper II) to OH/IR stars (Sloan et al. 2008) — the region of color space occupied by O-rich stars has been extended, increasing the overlap area between carbon-rich and oxygen-rich stars. The H II region area has also been expanded, to bluer J-K and K-A colors. The RSG region has been extended to redder K-A colors.

Those sources whose classifications were incorrect under the Paper II JHK8 system offer insight into the use of color-based diagnostics to identify the nature of objects. Many of these objects lie in overlap regions between diagnostic boxes or towards the edges of boxes. In particular, the revised JHK8 scheme presented here reveals larger overlap in color space between AGB stars of different dust chemistries (C-rich vs. O-rich), due to the inclusion of a handful of previously misclassified OH/IR stars. In the LMC, this overlap region is dominated by carbon stars (Fig. 8) as a consequence of the LMC’s low metallicity (Paper II), resulting in a relatively low JHK8 misclassification rate overall (\sim 20%). However, in the Milky Way and external galaxies of similar metallicity, more caution must be exercised in identifying the nature of sources as C-rich vs. O-rich AGB stars based on their JHKA colors alone. Furthermore, “contamination” of photometry or spectra due to crowded fields or surrounding H II regions confuses the classification of sources located in or near star-forming regions.

However, with the important exception of O-rich AGB stars with high mass loss rates (OH/IR stars) — which are likely to be present in larger proportion (relative to high mass loss rate carbon

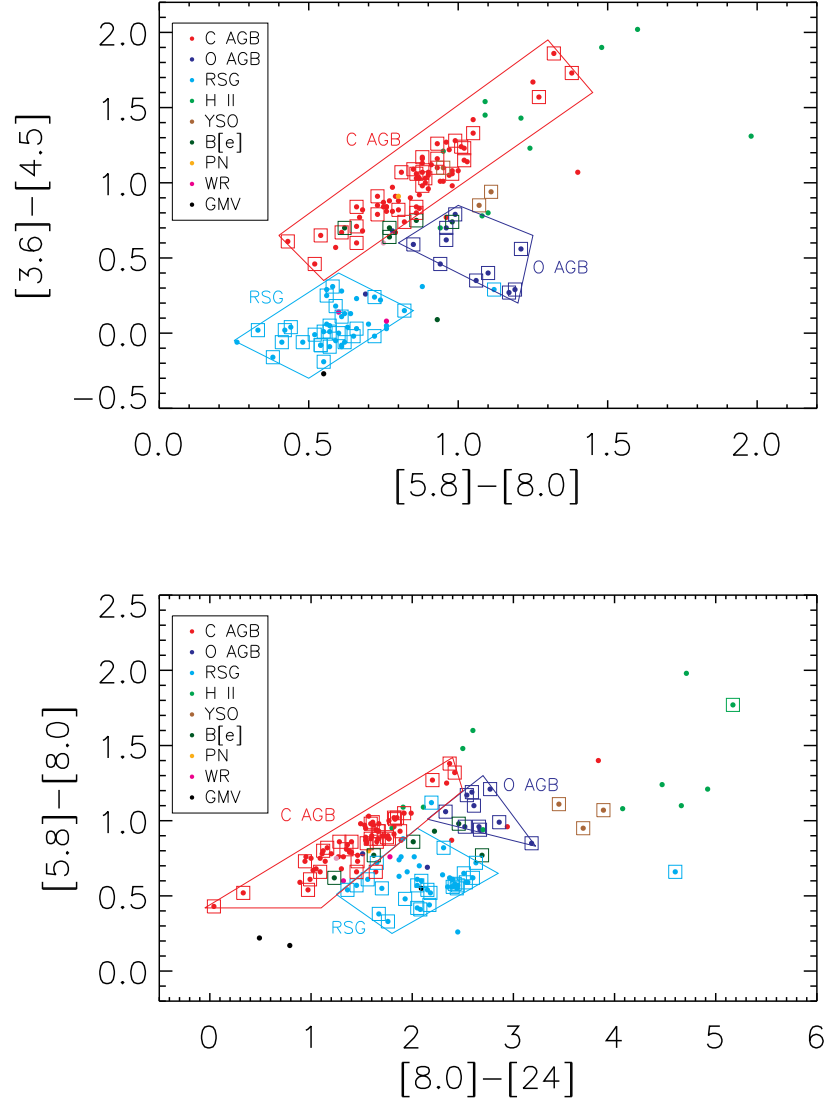


Fig. 9.— *Spitzer* IRAC/MIPS color-color diagrams for the whole sample of the 250 brightest $8\ \mu\text{m}$ sources in the LMC. Colors indicate the class of each object (from Paper II and Table 2). Open squares indicate objects whose classification is spectroscopically verified with IRS spectra. Boxes indicate the revised classification regions.

stars) in external galaxies with higher metallicity than that of the LMC – the results presented here indicate that the revised JHK8 color classification criteria can be used to classify the most luminous IR sources in nearby galaxies with $> 70\%$ confidence. These results therefore reinforce both the utility of the JHK8 color diagnostics and the conclusions in Paper II as to the preponderance of C-rich AGB stars and H II regions among most luminous IR sources in the LMC. In addition, the spectroscopic identifications found in this paper further reinforce the results of Paper II that *Spitzer* IRAC/MIPS color-color diagrams and IRAC/2MASS color-color diagrams can be used to distinguish between object classes. In particular, color-color diagrams that make use of *Spitzer* photometry appear to be far more effective in discriminating between O-rich and C-rich AGB stars than diagrams based solely on JHK8 colors.

This work is based on data from the *Spitzer* Space Telescope, which is operated by the Jet Propulsion Laboratory, California Institute of Technology under a contract with NASA. This research has made use of the SIMBAD database, operated at CDS, Strasbourg, France. We thank the anonymous referee for considered comments which improved this manuscript.

Facilities: Spitzer

REFERENCES

- Blum, R. D., et al. 2006, *AJ*, 132, 2034
- Buchanan, C. L., Kastner, J. H., Forrest, W. J., Hrivnak, B. J., Sahai, R., Egan, M., Frank, A., & Barnbaum, C. 2006, *AJ*, 132, 1890 (Paper I)
- Cannon, J. M., et al. 2006, *ApJ*, 652, 1170
- Egan, M. P., Van Dyk, S. D., & Price, S. D. 2001, *AJ*, 122, 1844 (EVP01)
- Goebel, J. H., & Moseley, S. H. 1985, *ApJ*, 290, L35
- Higdon, S. J. U. et al. 2004, *PASP*, 116, 975
- Hony, S., Waters, L. B. F. M., & Tielens, A. G. G. M. 2002, *A&A*, 390, 533
- Houck, J., et al. 2004, *ApJS*, 154, 18
- Jackson, D. C., Cannon, J. M., Skillman, E. D., Lee, H., Gehrz, R. D., Woodward, C. E., & Polomski, E. 2006, *ApJ*, 646, 192
- Jackson, D. C., Skillman, E. D., Gehrz, R. D., Polomski, E., & Woodward, C. E. 2007, *ApJ*, 667, 891
- Kastner, J. H., Buchanan, C. L., Sargent, B., & Forrest, W. J. 2006, *ApJ*, 638, L29
- Kastner, J. H., Thorndike, S. L., Romanczyk, P. A., Buchanan, C. L., Hrivnak, B. J., Sahai, R., & Egan, M. 2008, *AJ*, 136, 1221 (Paper II)
- Meixner, M., et al. 2006, *AJ*, 132, 2268
- Sloan, G. C., Kraemer, K. E., Wood, P. R., Zijlstra, A. A., Bernard-Salas, J., Devost, D., & Houck, J. R. 2008, *ApJ*, 686, 1056

- Smith, J. D. T., et al. 2007, *PASP*, 119, 1133
- Speck, A. K., Cami, J., Markwick-Kemper, C., Leisenring, J., Szczerba, R., Dijkstra, C., Van Dyk, S., & Meixner, M. 2006, *ApJ*, 650, 892
- van Loon, J. T., et al. 1998, *A&A*, 329, 169
- van Loon, J. T., et al. 2005, *MNRAS*, 364, L71
- Wood, P. R., Whiteoak, J. B., Hughes, S. M. G., Bessell, M. S., Gardner, F. F., & Hyland, A. R. 1992, *ApJ*, 397, 552
- Zijlstra, A. A., et al. 2006, *MNRAS*, 370, 1961

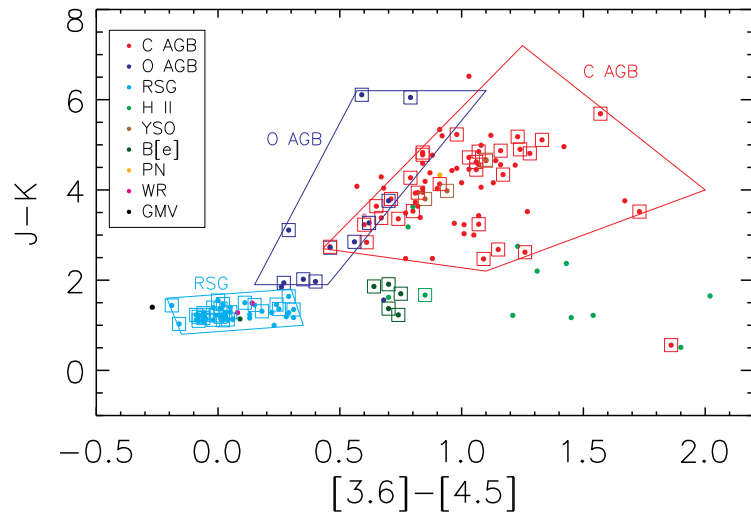


Fig. 10.— *Spitzer* IRAC and 2MASS J-K color-color diagram for the whole sample of the 250 brightest $8 \mu\text{m}$ sources in the LMC. Colors indicate the class of each object (from Paper II and Table 2). Open squares indicate objects whose classification is spectroscopically verified with IRS spectra. Boxes indicate classification regions defined from the spectroscopically verified objects.